BULLETIN OF THE POLISH ACADEMY OF SCIENCES
TECHNICAL SCIENCES
Vol. 56, No. 3, 2008

A novel phase-shift full-bridge converter with voltage-doubler and decoupling integrated magnetics in PV system

Y. JIANG[1*], Z. CHEN[2], J. PAN[1], X.I ZHAO[1], and P. LEE[1]

[1] Department of Electrical Engineering, Shanhai Jiao Tong University, Shanghai 200030, P.R. China
[2] Department of Electrical Engineering, Anhui University of Technology, Ma Anshan 243002, P.R. China

Abstract. A novel phase shift full bridge (PSFB) converter with voltage-doubler and decoupling integrated magnetics in photovoltaic (PV) systems is proposed. Considering the demand that the output voltage is higher than the input voltage in PV systems, the voltage-doubler is added to achieve higher voltage gain compared with the traditional PSFB. In order to avoid current oscillation caused by the voltage-doubler and obtain the wide zero voltage switching (ZVS) ranges, an external inductor is imposed on the circuit. Especially, to obtain much higher power density, the external inductor and transformer are integrated into one magnetic core. The operation and voltage gain of proposed converter are analyzed. Also, in order to reveal the effects the integrated magnetics gives to the converter, the decoupling condition and the expression of leakage inductor of integrated magnetics are obtained in detail. Finally a 100 W prototype converter is made and the experimental results are given to verify the analysis.

Key words: integrated magnetics, voltage-doubler, PSFB converter, PV system.

1. Introduction

Using the photovoltaic (PV) power system as an alternative energy resource has been widely discussed due to the rapid growth of power electronics techniques [1–3].There are three different systems widely used in PV applications – the centralized inverter system, the string inverter system, and the module integrated converter system [3, 4].The multi-string inverter is the further development of the string inverter, where several strings are interfaced with their own dc-dc converter to a common dc-ac inverter [5–9]. The main challenge is to develop a dc-dc converter that can lift the low voltage.

A Phase-Shift Full-Bridge (PSFB) converter is widely used for high voltage high power applications due to its advantages such as simple structure and zero-voltage switching (ZVS) [10–15]. However, full ZVS operation can only be achieved in a limited load and input-voltage range, unless a relatively large inductance is provided in series with the primary winding of the transformer which can be implemented by adding an external inductor. Several converters achieve ZVS in all primary switches over an extended load and input voltage range by utilizing energy stored in the inductive components of an auxiliary circuit [16–20]. Unfortunately, these converters are not appropriate to achieve high power density, high reliability, and low cost because of extra devices and/or complicated control circuitry.

In the modern power electronics industry the demand for integrated magnetics has become much stronger because of the following reasons [21–28]:

1) The number of magnetic components can be reduced.
2) The size and cost of power electronic circuits can be reduced.
3) Sometimes a controlled coupling between magnetic components is required to achieve special functions.

In brief, it is an effective method to improve power density.

When the PSFB converter is used in PV system as dc-dc converter, it has two main problems:

1) The voltage gain is higher, it means that the output voltage is much higher than the input voltage though the high voltage gain can be solved through the increasing of turns ratio of high-frequency transformer, it decreases the power density due to the increasing of the volume of transformer.
2) Due to the high voltage gain, the number of turns of secondary winding of transformer is more than that of primary winding of transformer, therefore, the leakage inductor of transformer used as resonant inductor to achieve wide ZVS range is not enough.

In this paper, in order to overcome above problems, a novel PSFB converter with voltage-doubler and decoupling integrated magnetics is proposed. The voltage-doubler is adopted to increase voltage gain. In order to avoid current oscillation that caused by the voltage source parallel with capacitors of voltage-doubler directly through transformer, an external inductor between voltage source and voltage-doubler is set. Moreover, the external inductor is also used as resonant inductor to achieve wide ZVS range, therefore, the problem that only leakage inductor of transformer is used to achieve wide ZVS range is not enough is solved. Especially, in order to improve power density and save volume of magnetics, the external inductor and transformer are integrated into one magnetic core. The integrated magnetics are decoupled in order not to

*e-mail: abjiangying@gmail.com

influence the operation of converter, and the leakage inductor of integrated magnetics is also used as resonant inductor to achieve ZVS besides the external inductor.

The paper studies the operation of the individual modes of the converter thoroughly. The key features in the individual modes are also discussed in detail. The theoretical analyses are done to explain the converter operations including the realization of ZVS and the calculation of voltage gain. Also, the decoupling condition of integrated magnetics is analyzed and the leakage inductor expression of integrated magnetics is obtained. Experimental results of a 100-W converter with 48-V input and 380-V output are provided at the end of the paper to confirm the theoretical analysis.

2. Operational principles

Figure 1 shows the circuit diagram of the conventional PSFB converter, in order to increase voltage gain and save volume of magnetics, conventional rectifier circuit is replaced by voltage-doubler, and resonant inductor L_r and transformer T are integrated into one magnetic core, the proposed converter is shown in Fig. 2. In Fig. 2 the winding of inductor L_r is in the left and right legs, and the winding of transformer T is in the middle leg. The operating waveforms of the proposed converter in the steady state are shown in Fig. 3.

In order to perform a mode analysis, several assumptions are made as follows:

1) Turns ratio of transformer T is n, and L_r includes leakage inductor.
2) Switches S_{1-4} are ideal except for parasitic capacitors ($C_{oss1} = C_{oss2} = C_{oss3} = C_{oss4} = C_{oss}$) and internal diodes ($D_1 = D_2 = D_3 = D_4$).
3) The output voltage V_0 is constant.
4) Voltage doubler is ideal, rectifier capacitors C_{r1} and C_{r2} are identical, and each voltage is $V_0/2$, D_{r1} and D_{r2} are rectifier diodes.

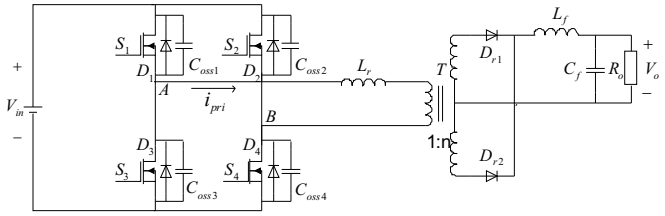

Fig. 1. Conventional PSFB converter

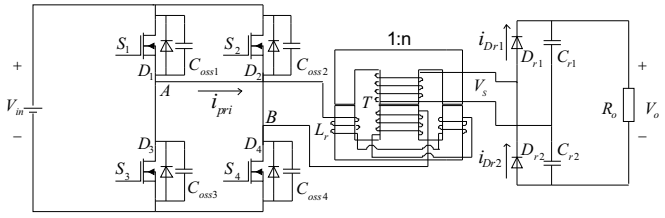

Fig. 2. Proposed PSFB converter with voltage-doubler and decoupling integrated magnetics

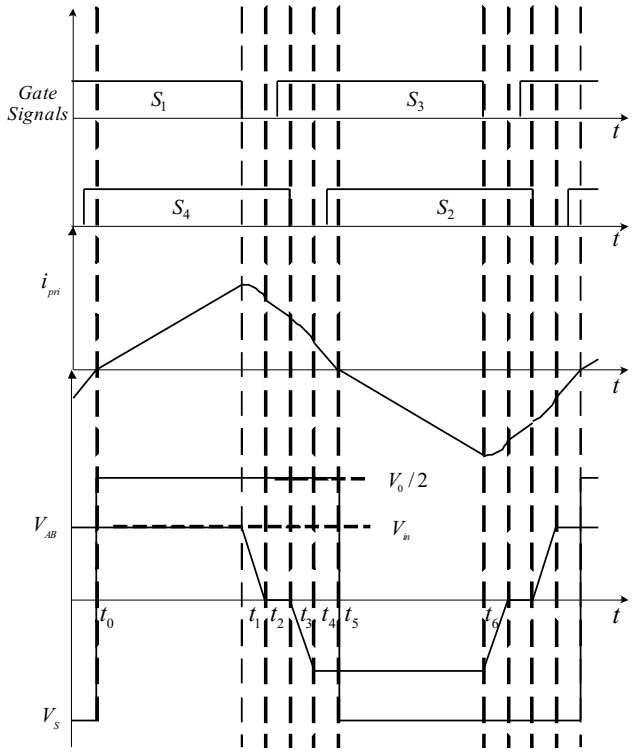

Fig. 3. Operating waveforms of the proposed converter

As shown in Fig. 3, each switching period is subdivided into six modes and their topological states are shown in Fig. 4. From t_0 to t_5, since the primary current $i_{pri}(t)$ and $i_{Dr1}(t)$ are continuous, that is, the voltage V_s of secondary side of transformer $T$is the voltage of C_{r1}, which means $V_s = V_0/2$.

1) Mode 1 ($t_0 - t_1$). The input power is transferred to the secondary side through S_1 and S_4. D_{r1} is turned on and C_{r1} is charged by $i_{Dr1}(t)$, therefore, the voltage $V_0/2n$ is reflected on the primary side of T, and $V_{in} - V_0/2n$ is put on L_r, that is, L_r determines the slope of the primary current $i_{pri}(t)$, and it can be described as follows:

$$i_{pri}(t) = \frac{V_{in} - V_o/2n}{L_r}(t - t_0). \tag{1}$$

2) Mode 2 ($t_1 - t_2$). When S_1 is turned off, C_{oss1} and C_{oss3} are charged and discharged by resonance with L_r respectively, and then the primary current $i_{pri}(t)$ and the voltage of C_{oss1} and C_{oss3} can be described as follows:

$$i_{pri}(t) = i_{pri}(t_1)\cos\omega(t - t_1) \tag{2}$$

$$v_{coss1}(t) = i_{pri}(t_1) \cdot Z \cdot \sin\omega(t - t_1) \tag{3}$$

$$v_{coss3}(t) = V_{in} - i_{pri}(t_1) \cdot Z \cdot \sin\omega(t - t_1) \tag{4}$$

where $\omega = \dfrac{1}{\sqrt{2C_{oss} \cdot L_r}}$, $Z = \sqrt{\dfrac{L_r}{2C_{oss}}}$.

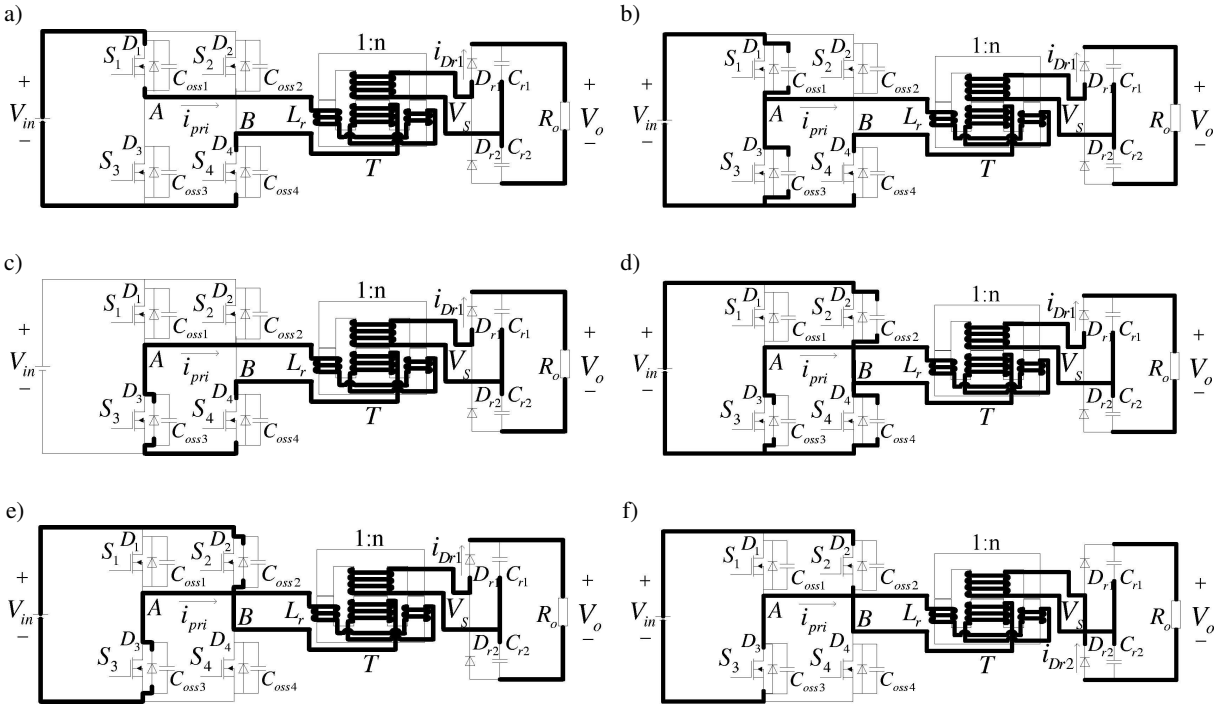

Fig. 4. Equivalent circuits of the proposed converter for mode analysis: (a) Mode 1, (b) Mode 2, (c) Mode 3, (d) Mode 4, (e) Mode 5, (f) Mode 6

3) Mode 3 ($t_2 - t_3$). The voltage of C_{oss3} is discharged to zero, the anti-diode D_3 of switch S_3 is turned on naturally, and then the S_3 can be turned on to achieve ZVS. The primary current $i_{pri}(t)$ can be described as follows:

$$i_{pri}(t) = i_{pri}(t_2) + \frac{-V_o/2n}{L_r}(t - t_2). \tag{5}$$

4) Mode 4 ($t_3 - t_4$). S_4 is turned off, C_{oss2} and C_{oss4} are discharged and charged by resonance with L_r respectively. Then the primary current$i_{pri}(t)$, and the voltage of C_{oss2} and C_{oss4} can be described as follows:

$$i_{pri}(t) = i_{pri}(t_3)\cos\omega(t - t_3) \tag{6}$$

$$v_{coss2}(t) = V_{in} - i_{pri}(t_3)\cdot Z\cdot\sin\omega(t - t_3) \tag{7}$$

$$v_{coss4}(t) = i_{pri}(t_3)\cdot Z\cdot\sin\omega(t - t_3) \tag{8}$$

where $\omega = \dfrac{1}{\sqrt{2C_{oss}\cdot L_r}}$, $Z = \sqrt{\dfrac{L_r}{2C_{oss}}}$.

5) Mode 5 ($t_4 - t_5$). The voltage of C_{oss2} is discharged to zero, the anti-diode D_2 of switch S_2 is turned on naturally, and then the S_2 can be turned on to achieve ZVS. The primary current $i_{pri}(t)$ can be described as follows:

$$i_{pri}(t) = i_{pri}(t_4) + \frac{-V_{in} - V_o/2n}{L_r}(t - t_4). \tag{9}$$

6) Mode 6 ($t_5 - t_6$). The primary current$i_{pri}(t)$ goes though S_2 and S_3, D_{r2} is turned on and C_{r2} is charged by $i_{Dr2}(t)$, therefore, the voltage $-V_0/2n$ is reflected on the primary side of T, and the analysis is similar with mode 1.

From mode 6, another circle is began which is similar with mode 1 to mode 5 analyzed above.

3. Analysis of voltage gain

Compared with conventional PSFB which is widely used to step down the input voltage, the proposed converter is used to lift input voltage. In order to analyze the voltage gain M (V_o/V_{in}), the waveform of primary current i_{pri} is shown in Fig. 5a. In Fig. 5a when $t_0 \le t \le t_1$, i_{pri} increases linearly as i^+_{pri}, when $t_1 \le t \le T$, i_{pri} decreases as i^-_{pri} which is composed of four parts which are described in formula (2), (5), (6), (9) respectively ($t_1 \le t \le t_2$, $t_2 \le t \le t_3$, $t_3 \le t \le t_4$, $t_4 \le t \le T$). Compared with mode 3 ($t_2 \le t \le t_3$) and mode 5($t_4 \le t \le T$), the charging and discharging time of mode 2($t_1 \le t \le t_2$) and mode 4($t_3 \le t \le t_4$) are instantaneous and then can be omitted, which are shown in Fig. 5b. In Fig. 5b i^-_{pri} is described as i^-_{pri1} ($t_{on} \le t \le t_{off}$) and i^-_{pri2} ($t_{off} \le t \le T$), $I_{\max}$ and I_{av} are, respectively, the max value of i_{pri} and the average value of i_{pri}. I_{av} can be described as follows:

$$I_{av}T = \int_0^{t_{on}} i^+_{pri}dt + \int_{t_{on}}^{t_{off}} i^-_{pri1}dt + \int_{t_{off}}^{T} i^-_{pri2}dt \tag{10}$$

i^+_{pri}, i^-_{pri1} and i^-_{pri2} can be described as follows:

$$\begin{cases} i^+_{pri} = \dfrac{V_{in} - V_o/2n}{L_r}(t - t_0) \\ i^-_{pri1} = i^+_{pri}(t_{on}) + \dfrac{-V_o/2n}{L_r}(t - t_{on}) \\ i^-_{pri2} = i^-_{pri1}(t_{off}) + \dfrac{-V_{in} - V_o/2n}{L_r}(t - t_{off}) \end{cases}. \tag{11}$$

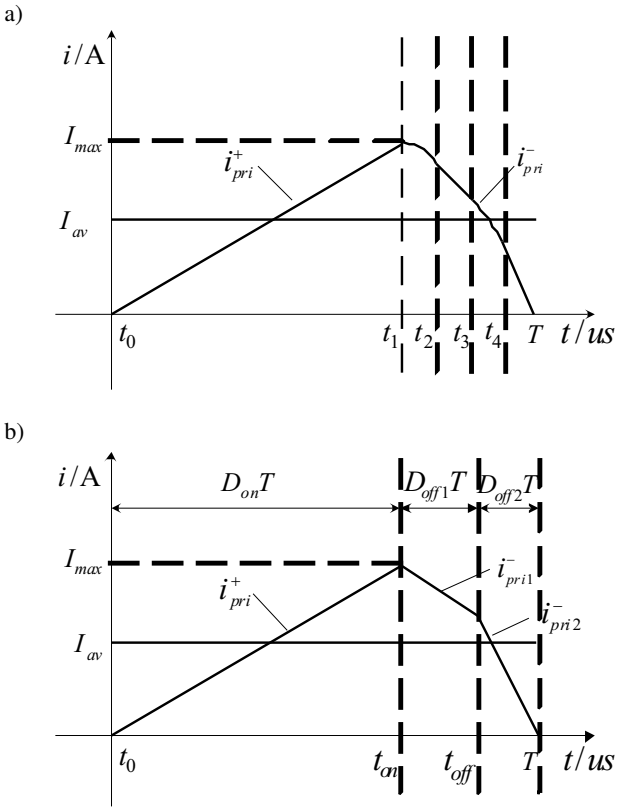

Fig. 5. Waveforms of primary current: (a) waveform of primary current, (b) simplified waveform of primary current

Based on power conservation, I_{av} also can be described as follows:

$$I_{av} = \frac{V_o^2}{V_{in}R}. \tag{12}$$

Based on (10), (11), (12), the voltage gain M (V_o/V_{in}) can be got as follows:

$$M = \frac{V_o}{V_{in}} = \frac{D_2}{\frac{1}{4n} + \frac{1}{2}\sqrt{\frac{1}{4n^2} + 4\frac{L_r f}{R}D_1}} \tag{13}$$

where $D_{on}T = t_{on} - t_0$, $D_{off1}T = t_{off} - t_{on}$, $D_{off2}T = T - t_{off}$, $f = 1/T$, R is load,

$$\begin{cases} D_1 = \dfrac{\frac{1}{2}D_{on}^2 + \frac{1}{2}D_{off2}^2 + D_{on}D_{off1}}{\left(\frac{1}{2}D_{on}^2 + \frac{1}{2}D_{off1}^2 + D_{on}D_{off1} - \frac{1}{2}D_{off2}^2\right)^2} \\ D_2 = \dfrac{\frac{1}{2}D_{on}^2 + \frac{1}{2}D_{off2}^2 + D_{on}D_{off1}}{\frac{1}{2}D_{on}^2 + \frac{1}{2}D_{off1}^2 + D_{on}D_{off1} - \frac{1}{2}D_{off2}^2} \end{cases}. \tag{14}$$

From (13) and (14), it can be got that voltage gain M is decided by D_1, D_2, turns ratio n, resonant inductor L_r, frequency f and load R. It means that such parameters should be adjusted together to satisfy the voltage gain M demanded.

4. Design of integrated magnetics

4.1. Decoupling of integrated magnetics. The proposed PSFB converter is used to lift voltage, which means that the number of turns of transformer primary winding is less than that of transformer secondary winding. Furthermore, the leakage inductor in primary winding is much smaller, therefore, the ZVS range is narrow when only the leakage inductor is used for resonance. In order to solve this problem, an external inductor is added, but it increases volume which results in the decreasing of power density. In this paper, the integrated magnetics which are shown in Fig. 6 are used to solve this problem. In Fig. 6a transformer T and inductor L_r are integrated into one EE magnetic core, N_P and N_S are, respectively, the number of turns of primary winding and secondary winding of transformer T, N_{L1} and N_{L2} are the number of turns of inductor L_r, $\Re_1$, $\Re_{21}$ and $\Re_{22}$ are, respectively, the magnetic resistance in middle leg, left leg and right leg, i_P, i_s and i_L are, respectively, the current of primary winding, secondary winding and inductor L_r, the transformer winding is in the middle leg, and the inductor winding is divided into two parts which are in left and right legs respectively, φ_{TL1} and φ_{TL2} are, respectively, the fluxes in transformer windings (middle leg) which are imposed by inductor winding (left and right legs), φ_{LT1} and φ_{LT2} are, respectively, the fluxes in inductor winding which are imposed by transformer winding, and the magnetic circuit is shown in Fig. 6b. In order to prevent their fluxes from coupling with each other, which make it difficult to analyze the operation of converter, the integrated magnetics are decoupled.

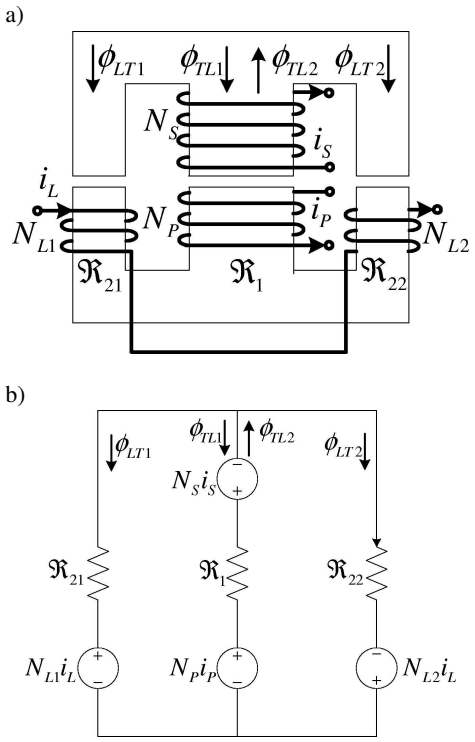

Fig. 6. Integrated magnetics: (a) integrated transformer and inductor, (b) equivalent magnetic circuit

Based on Fig. 6b, the fluxes φ_{TL1} and ϕ_{TL2} can be described as follows:

$$\begin{cases} \phi_{TL1} = \dfrac{N_{L1} i_L \Re_{22}}{\Re_1\Re_{21} + \Re_1\Re_{22} + \Re_{21}\Re_{22}} \\ \phi_{TL2} = \dfrac{N_{L2} i_L \Re_{21}}{\Re_1\Re_{21} + \Re_1\Re_{22} + \Re_{21}\Re_{22}} \end{cases}. \tag{15}$$

The flux linkage ψ_{TL} of transformer T which is imposed by inductorL_r is described as follows:

$$\psi_{TL} = (N_P - N_S)(\phi_{TL1} - \phi_{TL2}) = \frac{N_P i_L - N_S i_L}{\Re_1\Re_{21} + \Re_1\Re_{22} + \Re_{21}\Re_{22}}(N_{L1}\Re_{22} - N_{L2}\Re_{21}). \tag{16}$$

The fluxes ϕ_{LT1} and ϕ_{LT2} can be described as follows:

$$\begin{cases} \phi_{LT1} = \dfrac{(N_P i_P - N_S i_S)\Re_{22}}{\Re_1\Re_{21} + \Re_1\Re_{22} + \Re_{21}\Re_{22}} \\ \phi_{LT2} = \dfrac{(N_P i_P - N_S i_S)\Re_{21}}{\Re_1\Re_{21} + \Re_1\Re_{22} + \Re_{21}\Re_{22}} \end{cases}. \tag{17}$$

The flux linkage ψ_{LT} of inductor L_r which is imposed by transformer T is described as follows:

$$\psi_{LT} = N_{L1}\phi_{LT1} - N_{L2}\phi_{LT2} = \frac{N_P i_P - N_S i_S}{\Re_1\Re_{21} + \Re_1\Re_{22} + \Re_{21}\Re_{22}}(N_{L1}\Re_{22} - N_{L2}\Re_{21}) \tag{18}$$

When $\psi_{LT} = \psi_{TL} = 0$, the inductor L_r and transformer T are decoupled, the decoupling condition can be got as follow from (16) and (18):

$$\frac{\Re_{21}}{\Re_{22}} = \frac{N_{L1}}{N_{L2}}. \tag{19}$$

In order to design it conveniently, make air gaps of left leg and right leg be the same, which means that $\Re_{21} = \Re_{22}$, and then the condition of decoupling is got from (19):

$$N_{L1} = N_{L2}. \tag{20}$$

Assuming that B_1, B_{21} and B_{22} are, respectively, the flux density of middle leg, left leg and right leg, they can be described as follows:

$$\begin{cases} B_1 = \dfrac{(N_P i_P - N_S i_S)(\Re_{21} + \Re_{22})}{(\Re_1\Re_{21} + \Re_1\Re_{22} + \Re_{21}\Re_{22})S_1} \\ B_{21} = \dfrac{i_L(N_{L1} + N_{L2})}{(\Re_{21} + \Re_{22})S_{21}} - \dfrac{(N_P i_P - N_S i_S)\Re_{22}}{(\Re_1\Re_{21} + \Re_1\Re_{22} + \Re_{21}\Re_{22})S_{21}} \\ B_{22} = \dfrac{i_L(N_{L1} + N_{L2})}{(\Re_{21} + \Re_{22})S_{22}} + \dfrac{(N_P i_P - N_S i_S)\Re_{21}}{(\Re_1\Re_{21} + \Re_1\Re_{22} + \Re_{21}\Re_{22})S_{22}} \end{cases} \tag{21}$$

where S_1, S_{21} and S_{22} are, respectively, the cross section areas of middle leg, left leg and right leg.

The integrated magnetics are designed to make sure that each leg is not saturated according to (21).

4.2. Leakage inductor of integrated magnetics. Compared with conventional PSFB converter which adopts leakage inductor of transformer as resonant inductor, the proposed PSFB converter's resonant inductor includes two parts: (1) Inductor L_r integrated in magnetics. (2) Leakage inductor of integrated magnetics. Therefore, it is necessary to analyze the leakage inductor of integrated magnetics.

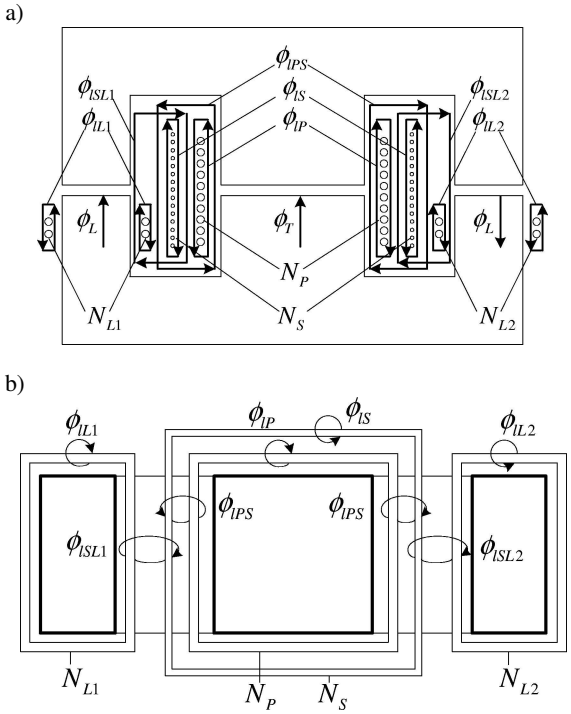

Fig. 7. Leakage flux of integrated magnetics: (a) front view of integrated magnetics, (b) top view of integrated magnetics

The leakage fluxes of integrated magnetics are shown in Fig. 7, V_L, V_P and V_S are, respectively, the voltage of inductor winding, primary winding of transformer T, and secondary winding of transformer T, they can be described as follows:

$$\begin{cases} V_L = N_L \dfrac{d}{dt}(\phi_L + \phi_{lL} + \phi_{lSL1} + \phi_{lSL2}) \\ V_P = N_P \dfrac{d}{dt}(\phi_T + \phi_{lP} + \phi_{lPS}) \\ V_S = N_S \dfrac{d}{dt}(-\phi_T + \phi_{lS} - \phi_{lPS} + \phi_{lSL1} - \phi_{lSL2}) \end{cases} \tag{22}$$

where N_L ($N_L = N_{L1} + N_{L2}$) is the number of turns of inductor L_r, ϕ_T and ϕ_L are, respectively, the fluxes of transformer T and inductor L_r. ϕ_{lL}, ϕ_{lP} and ϕ_{lS} are, respectively, the leakage fluxes of inductor winding, primary winding and secondary winding of transformer T, ϕ_{lSL1}, ϕ_{lSL2} and ϕ_{lPS} are, respectively, the leakage fluxes which goes through inductor winding in left leg and secondary winding of transformer T, inductor winding in right leg and secondary winding of transformer T, and primary winding and secondary winding of transformer T, and they can be described as follows:

$$\begin{cases} \phi_T = \dfrac{(N_P i_P - N_S i_S)(\Re_{21} + \Re_{22})}{(\Re_1\Re_{21} + \Re_1\Re_{22} + \Re_{21}\Re_{22})} \\ \phi_L = \dfrac{N_L i_L}{\Re_{21} + \Re_{22}} \\ \phi_{lSL1} = \dfrac{N_{L1} i_L + N_S i_S}{\Re_{lSL1}}, \phi_{lSL2} = \dfrac{N_{L2} i_L - N_S i_S}{\Re_{lSL2}} \\ \phi_{lPS} = \dfrac{N_P i_P - N_S i_S}{\Re_{lPS}} \\ \phi_{lL} = \dfrac{N_L i_L}{\Re_{lL}}, \phi_{lP} = \dfrac{N_P i_P}{\Re_{lP}}, \phi_{lS} = \dfrac{N_S i_S}{\Re_{lS}} \end{cases} . \quad (23)$$

where, $\Re_{lijk}$ is leakage magnetic resistance according to its corresponding leakage flux ϕ_{lijk}, $i = L, S, P$, $j = L, S, P$, $k = 1, 2$.

Further more, in order to get the expression of leakage inductor, the formula (22) can be deduced as follows:

$$\begin{pmatrix} V_L \\ V_P \\ V_S \end{pmatrix} = \begin{pmatrix} L_L + L_{lL} + L_{lL1} + L_{lL2} & 0 & M_{lL1} - M_{lL2} \\ 0 & L_P + L_{lP} + L_{lPS} & -M_{lPS} - M_{PS} \\ M_{lS1} - M_{lS2} & -M_{lSP} - M_{SP} & L_S + L_{lS} + L_{lSP} + L_{lS1} + L_{lS2} \end{pmatrix} \begin{pmatrix} \dfrac{di_L}{dt} \\ \dfrac{di_P}{dt} \\ \dfrac{di_S}{dt} \end{pmatrix} \quad (24)$$

where

$$\begin{cases} L_L = \dfrac{N_L^2}{\Re_{21} + \Re_{22}}, L_{lL} = \dfrac{N_L^2}{\Re_{lL}}, \\ L_{lL1} = \dfrac{N_L^2}{2\Re_{lSL1}}, L_{lL2} = \dfrac{N_L^2}{2\Re_{lSL2}} \\ M_{lL1} = \dfrac{N_L N_S}{2\Re_{lSL1}}, M_{lL2} = \dfrac{N_L N_S}{2\Re_{lSL2}}; \\ L_P = \dfrac{N_P^2(\Re_{21} + \Re_{22})}{\Re_1\Re_{21} + \Re_1\Re_{22} + \Re_{21}\Re_{22}}, \\ L_{lP} = \dfrac{N_P^2}{\Re_{lP}}, L_{lPS} = \dfrac{N_P^2}{\Re_{lPS}} \\ M_{lPS} = \dfrac{N_P N_S}{\Re_{lPS}}, \\ M_{PS} = \dfrac{N_P N_S(\Re_{21} + \Re_{22})}{\Re_1\Re_{21} + \Re_1\Re_{22} + \Re_{21}\Re_{22}}; \\ L_S = \dfrac{N_S^2(\Re_{21} + \Re_{22})}{\Re_1\Re_{21} + \Re_1\Re_{22} + \Re_{21}\Re_{22}}, L_{lS} = \dfrac{N_S^2}{\Re_{lS}}, \\ L_{lSP} = \dfrac{N_S^2}{\Re_{lPS}}, L_{lS1} = \dfrac{N_S^2}{\Re_{lSL1}}, L_{lS2} = \dfrac{N_S^2}{\Re_{lSL2}} \\ M_{lS1} = \dfrac{N_L N_S}{\Re_{lSL1}}, M_{lS2} = \dfrac{N_L N_S}{\Re_{lSL2}}, M_{lSP} = \dfrac{N_P N_S}{\Re_{lPS}}, \\ M_{SP} = \dfrac{N_P N_S(\Re_{21} + \Re_{22})}{\Re_1\Re_{21} + \Re_1\Re_{22} + \Re_{21}\Re_{22}} \end{cases} . \quad (25)$$

The total leakage inductor L_l for resonance can be described as follows:

$$L_l = L_{Ll} + L_{TPl} + \frac{N_P^2}{N_S^2} L_{TSl} \quad (26)$$

where, $L_{Ll}$is total leakage inductor of the inductorL_r. $L_{TPl}$and$L_{TSl}$are, respectively, the total leakage inductor of primary and secondary winding of transformer$T$, and they can be described as follows:

$$\begin{cases} L_{Ll} = L_{lL} + L_{lL1} + L_{lL2} + M_{lL1} - M_{lL2} \\ L_{TPl} = L_{lP} + L_{lPS} - M_{lPS} \\ L_{TSl} = M_{lS1} - M_{lS2} + L_{lS} + L_{lSP} + L_{lS1} + L_{lS2} - M_{lSP} \end{cases} . \quad (27)$$

Since leakage magnetic resistance $\Re_{lSL1}$ equates to $\Re_{lSL2}$ approximately, and then $M_{lL1} = M_{lL2}$, $M_{lS1} = M_{lS2}$, the formula (27) can be simplified as follows:

$$\begin{cases} L_{Ll} = L_{lL} + L_{lL1} + L_{lL2} \\ L_{TPl} = L_{lP} + L_{lPS} - M_{lPS} \\ L_{TSl} = L_{lS} + L_{lSP} + L_{lS1} + L_{lS2} - M_{lSP} \end{cases} . \quad (28)$$

According to (28), L_{Ll} is only composed of its self leakage inductors, since the mutual leakage inductors M_{lL1} and M_{lL2} between inductor L_r and transformer T are counteracted by each other, it isn't influenced by transformer. The leakage inductor of transformer T is composed of L_{TPl} and L_{TSl}, since the mutual leakage inductors M_{lS1} and M_{lS2} between L_r and transformer T are counteracted by each other, it isn't influenced by inductor L_r. Therefore, besides the fluxes between inductor L_r and transformer T, the leakage fluxes between them are also decoupled. The decoupling integrated magnetics can be seen as discrete inductor L_r and transformer T, and then the leakage inductors can be measured by common short experiment.

5. Experimental results

5.1. Decoupling of integrated magnetics. The parameters of integrated magnetics are shown as follows: the resonant inductor is $L_r = 12.5$ uH, the inductor of transformer primary winding is $L_{TP} = 138$ uH, the inductor of transformer secondary winding is $L_{TS} = 2.8$ mH, the leakage inductor of transformer primary winding is $L_{TPl} = 2.1$ uH, the leakage inductor of transformer secondary winding is $L_{TSl} = 42$ uH, the turns ratio is $N_S : N_P = 4.5$, the air gaps of three legs are the same are $0.4mm$. L_{TPl} and L_{TSl} are measured by short circuit experiment, since L_r less than 10% of L_{TP}, compared with L_{TPl}, L_{Ll} is so small that it can be omitted. Based on (26) it can be calculated that $L_l = 4.2$ uH. In order to test the decoupling of integrated magnetics, a 5 V and 100 Khz sinusoidal voltage source is imposed on integrated magnetics. When voltage source is imposed on the primary winding of transformer T, the waveform of the voltage of transformer secondary side v_s and inductor v_l are shown

in Fig. 8a. In Fig. 8a v_s is 22.6 V according to turns ratio, and v_l is zero approximately, it means that the voltages of transformer and inductor don't influence on each other due to decoupling. When voltage source is imposed on the inductor winding, the waveform of the voltage of transformer secondary side v_s and primary side v_p are shown in Fig. 8b. In Fig. 8b if inductor and transformer are coupled closely, according to turns ratio ($N_L : N_P = \sqrt{L_{TP}/L_r} = 3.3$ and $N_L : N_S = \sqrt{L_{TS}/L_r} = 14.8$) v_p should be 16.5 V and v_s should be 74 V, from Fig. 8b it can be seen that v_p and v_s are less than 10% of 16.5 V and 74 V, therefore, inductor and transformer are decoupled with each other approximately.

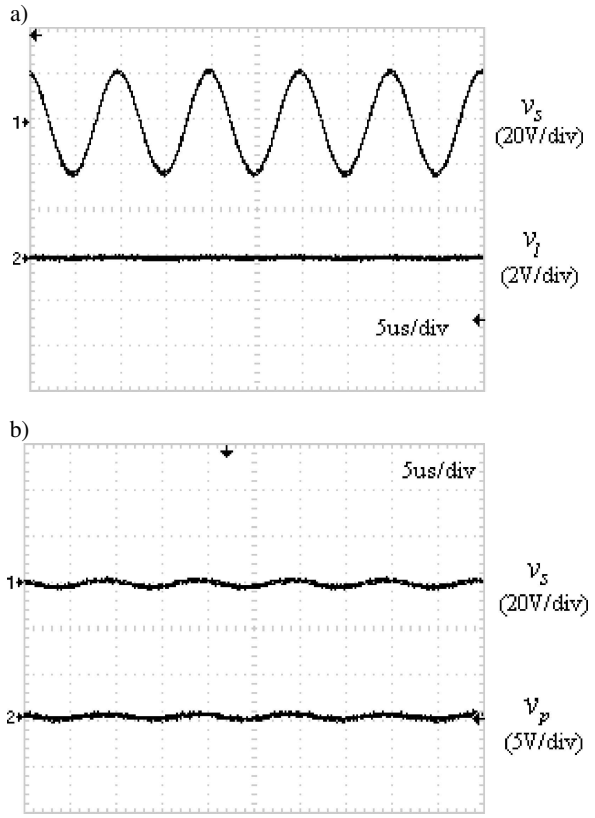

Fig. 8. Waveforms of decoupling integrated magnetics: (a) waveforms of v_s and v_l, (b) waveforms of v_p and v_s

5.2. PSFB converter. Based on the designed parameters, a 100 kHz, 100 W, 380 V prototype dc-dc power module with an input voltage range of 48 V has been constructed. The parameters are as follows: IRF3815s and BYM36Cs are used as switching devices and voltage-double diodes, voltage-double capacitors are selected as 0.1 uF. The key experimental waveforms are shown in Figs. 9–13, it can be seen that all the waveforms agree well with the theoretical analysis. Figure 9 shows the primary current i_{pri} with different L_r. In Fig. 9a when $L_r = 7.3$ uH the i_{pri} decreases to zero before next circle due to the small L_r, therefore, the oscillation of i_{pri} is caused. In Fig. 9b and c, with the increasing of L_r the i_{pri} becomes continuous, the oscillation of i_{pri} is reduced, and the ZVS range is widen. Figure 10 shows the waveform of v_{AB}, when v_{AB} becomes zero the leading switches can achieve ZVS. Figure 11 shows the waveforms of lagging switch, it can be seen that when gate signal v_{GS} is on, the voltage of switch v_{DS} has been decreased to zero, and then the lagging switch achieves ZVS. Figures 12–13 show the waveforms of v_{TS} and the voltage v_{Cr1} and v_{Cr2} of voltage-doubler, when v_{Cr1} is charged v_{TS} equates to v_{Cr1}, when v_{Cr2} is charged v_{TS} equates to v_{Cr2} since $V_o = v_{Cr1} + v_{Cr2}$, the output voltage V_o doubled the v_{TS}. Figure 14 shows the converter efficiencies under some load conditions. Figure 15 shows the photograph of Prototype 100-W converter.

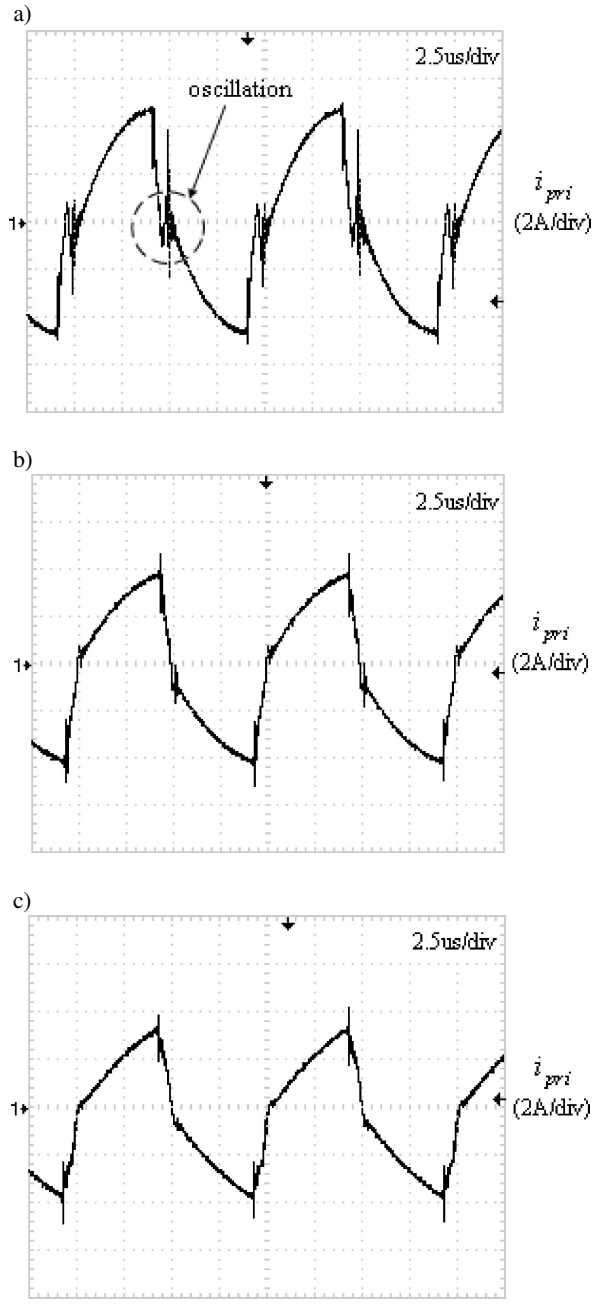

Fig. 9. Waveforms of i_{pri} with different L_r: (a) $L_r = 7.3$ uH, (b) $L_r = 12.5$ uH, (c) $L_r = 17.6$ uH

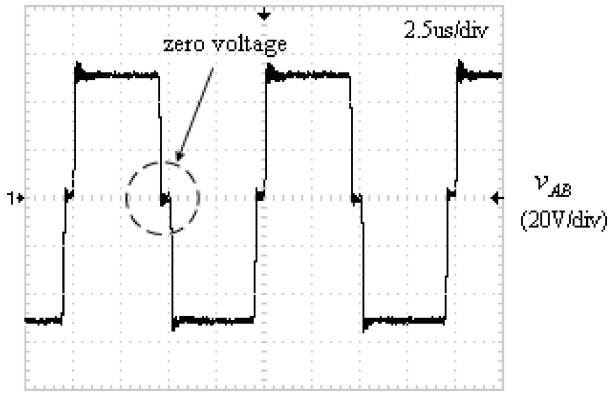

Fig. 10. Waveform of v_{AB}

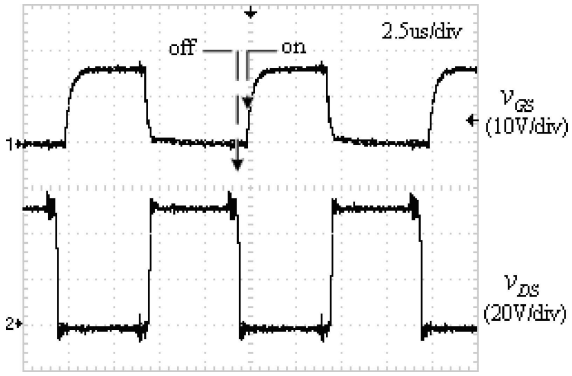

Fig. 11. Waveforms of lagging switch

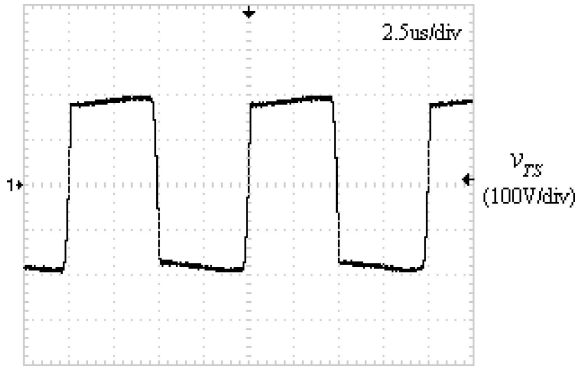

Fig. 12. Waveform of v_{TS}

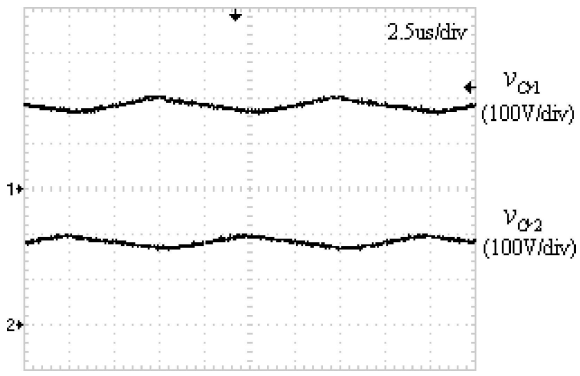

Fig. 13. Waveforms of voltage-doubler

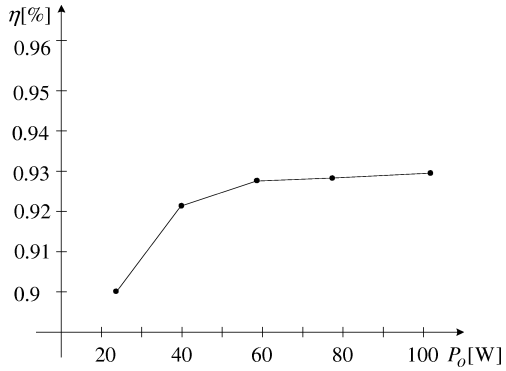

Fig. 14. The converter efficiencies under a range of load conditions

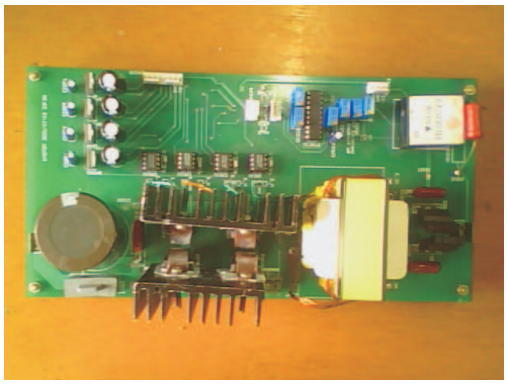

Fig. 15. Prototype 100-W converter

6. Conclusions

In this paper, a novel PSFB converter with voltage-doubler and integrated magnetics in PV system is proposed. The voltage-doubler is adopted to increase voltage gain and an external inductor which is used not only to avoid current oscillation but also as resonant inductor to achieve ZVS is added. Especially, the external inductor and transformer are integrated into one magnetic core to improve power density. The operational principles have been presented by the mode analysis, and the design equations for the achievement of ZVS and the voltage gain are derived. Moreover, the decoupling condition of integrated magnetics and the leakage inductor expression of integrated magnetics are obtained. Based on the design of ZVS, voltage gain and integrated magnetics, a prototype has been designed to prove the validity of the proposed converter. The experimental results of a 100 W prototype converter have been presented. The efficiency of the proposed converter is obtained about 93% at a rated condition.

The proposed converter is suitable for the multi-string inverter as dc-dc converter in PV system requiring the high efficiency and high power density.

REFERENCES

[1] S.B. Kjær, J.K. Pedersen, and F. Blaabjerg, "Power inverter topologies for photovoltaic modules – a review", *Proc. IEEE IAS'02 Conf.*, 782–788 (2002).

[2] F. Blaabjerg, Z. Chen, and S.B. Kjær, "Power electronics as efficient interface in dispersed power generation systems," *IEEE Trans. Power Electron.* 19 (5), 1184–1194, (2004).

[3] S.B. Kjær, J.K. Pedersen, and F. Blaabjerg, "A review of single-phase grid-connected inverters for photovoltaic modules", *IEEE Trans. Ind. Appl.* 41 (5) 1292–1306 (2005).

[4] Z. Chen, X. Zhang, and J. Pan. "An integrated inverter for a single-phase single-stage grid-connected PV system based on Z-source", *Bull. Pol. Ac.: Tech.* 55 (3), 263–272 (2007).

[5] B. Verhoeven, "Utility aspects of grid connected photovoltaic power systems", *Int. Energy Agency Photovoltaic Power Systems* IEA PVPS T5-01, www.iea-pvps.org (1998).

[6] M. Meinhardt and G. Cramer, "Past, present and future of grid connected photovoltaic- and hybrid-power-systems", *Proc. IEEE-PES Summer Meeting* 2, 1283–1288 (2000).

[7] Ruszczyk, "Minimization current error area of the DC/AC inverter controlled by predictive current control method", *Bull. Pol. Ac.: Tech.* 54 (3), 279–286 (2006).

[8] Sunny Boy, *5000TL Multi-String – Operating Instructions, SMA*, www.sma.de (2005).

[9] P. Antoniewicz and M.P. Kazmierkowski, "Predictive direct power control of three-phase boost rectifier", *Bull. Pol. Ac.: Tech.* 54 (3), 287–292 (2006).

[10] J.A. Sabate, V. Vlatkovic, R.B. Ridley, F.C. Lee, and B.H. Cho, "Design considerations for high-voltage high-power full-bridge zero voltage- switched PWM converter", *Proc. IEEE APEC'90* 275–284 (1990).

[11] L.H. Mweene, C.A. Wright, and M.F. Schlecht, "A 1 kW 500 kHz front-end converter for a distributed power supply system", *IEEE Trans. Power Electron.* 6 (3), 398–407 (1991).

[12] D.B. Dalal, "A 500 kHz multi-output converter with zero voltage switching", *Proc. IEEE APEC'90 Conference*, 265–274 (1990).

[13] R. Redl, N.O. Sokal, and L. Balogh, "A novel soft-switching full-bridge dc/dc converter: analysis, design considerations, and experimental results at 1.5 kW, 100 kHz", *Proc. IEEE PESC'90 Conference*, 162–172 (1990).

[14] J.A. Sabaté, V. Vlatkovic', R.B. Ridley, and F.C. Lee, "High-voltage, high-power, ZVS, full-bridge PWM converter employing an active snubber", *Proc. IEEE APEC'91 Conference*, 158–163 (1991).

[15] W. Chen, F.C. Lee, M.M. Jovanovic', and J.A. Sabaté, "A comparative study of a class of full bridge zero-voltage-switched PWM converters", *Proc. IEEE APEC'95 Conference* 893–899, (1995).

[16] Y. Jang, M.M. Jovanovic', and Y. Ming Chang, "A new ZVS-PWM full-bridge converter", *IEEE Trans. Power Electron.* 18, 1122–1129 (2003).

[17] M. Nakaoka, S. Nagai, Y.J. Kim, Y. Ogino, and Y. Murakami, "The state-of-the art phase-shifted ZVS-PWM series & parallel resonant dc-dc power converters using internal parasitic circuit components and new digital control", *Proc. IEEE PESC'92 Conf.* 62–70 (1992).

[18] P.K. Jain, W. Kang, H. Soin, and Y. Xi, "Analysis and design considerations of a load and line independent zero voltage switching full bridge dc/dc converter topology", *IEEE Trans. Power Electron.* 17, 649–657 (2002).

[19] J.G. Cho, J.A. Sabaté, and F.C. Lee, "Novel full bridge zero-voltage transition\PWM dc/dc converter for high power application", *Proc.IEEE APEC'94 Conf.* 143–149 (1994).

[20] R. Ayyanar and N. Mohan, "Novel soft-switching dc-dc converter with full ZVS-range and reduced filter requirement – part I: regulated-output applications", *IEEE Trans. Power Electron.* 16, 184–192 (2001).

[21] G.B. Crouse, "Electrical filter", *U.S. Patent* 1 920 948 (1933).

[22] A. Lloyde, "Choking up on LC filters", *Electron. Mag* 40 (17), 93–97 (1967).

[23] J. Cielo and H. Hoffman, "Combined transformer and inductor device", *U.S. Patents* 3 553 620, and 3 694 726 (1972).

[24] G.C. Waehner, "Switching power supply common output filter", *U.S. Patent* 3 916 286 (1975).

[25] S. Cuk, "DC-to-DC switching converter with zero input & output ripple and integrated magnetics circuits", *U.S. Patent* 4 257 087 (1981).

[26] G.E. Bloom, "New integrated-magnetic DC-DC power converter circuitsand systems", *IEEE Trans. Magnetics* 39 (2), 57–66 (2003).

[27] M. Archer, "Integrated magnetic resonant power converter", *U.S. Patent* 4 774 649 (1988).

[28] P.W. Lee, Y.S. Lee, D.K.W. Cheng, and X.C. Liu, "Steady-state analysis of an interleaved boost converter with coupled inductors", *IEEE Trans. Ind. Electron* 47, 787–795 (2000).